Received 00th January 20xx,
Accepted 00th January 20xx

DOI: 10.1039/x0xx00000x

www.rsc.org/

Rapid catalysis carbonization and N-doping for the synthesis of hierarchical porous carbon as an efficient metal-free catalyst for oxygen reduction reaction

Li-Yuan Zhang,[a] Meng-Ran Wang,[b] Yan-Qing Lai,[b] Xiao-Yan Li[a,*]

Abstract. A high-performance, durable, and inexpensive metal-free catalyst for oxygen reduction reaction (ORR) is an attractive candidate to replace Pt-based materials in fuel cells, but its production is still a major challenge. In this study, we developed a fast catalysis carbonization process, followed by N-doping for activation, to synthesize high-performance porous carbon as the metal-free catalyst using waste banana peel as the carbon source. The C conversion efficiency of the new method reached as high as 41.9%. The $ZnCl_2$-based fast catalysis carbonization process requires only 25 min, which includes heating and cooling, and can be operated almost continuously, which is highly favorable for large-scale and effective production. The carbon products were then doped by N (to ~3 at.%) using melamine to enable important features, such as a high specific surface area (~1097 $m^2 g^{-1}$) and a hierarchical porous structure with abundant micropores. Compared to commercial Pt/C materials, the as-prepared carbon catalyst exhibits a comparable electrocatalytic activity and much better stability. This novel technique can also be readily applied to produce metal-free carbon catalysts from other waste biomass (e.g., orange peel, leaves) as the carbon sources. The method can be developed as a general and effective industrial route to transform waste biomass into high value-added hierarchical porous carbon with superior functionalities.

1. Introduction

Research into the development of alternative and sustainable energy sources has become an urgent task, due to the increasing consumption of non-renewable fossil fuels and the related environmental problems (e.g., air pollution, greenhouse gas emission, and subsequent global warming).[1-3] In this context, fuel cells with high energy density and sustainable features are of particular interest.[4, 5] The conversion efficiency of fuel cells is, however, commonly limited by slow oxygen reduction reaction (ORR) at the cathode, due to the high activation energy of the reaction.[6-8] The activation energy can be reduced with the aid of catalysts, and currently noble metals-based catalysts, typically Pt-based materials,[11-13]are commonly used,[9, 10] but unfortunately these suffer not only from poor stability in various fuel cell conditions but also from a poor tolerance to methanol.[14, 15] Not to mention that noble metals are also scarce and expensive. A United States Department of Energy study found that Pt-based catalysts account for ~50% of the total cost of fuel cells.[16, 17] Thus, developing low-cost catalysts with a high ORR efficiency, reliable methanol tolerance, and potential of large-scale production is essential for fuel cell technology, but it remains a great challenge.[18-21]

Carbonaceous materials are low-cost and possess high biocompatibility and electrocatalytic activity,[22-24] making them a suitable metal-free catalyst that can replace Pt-based materials.[25-28] Waste biomass-derived carbon has thus attracted increasing attention, due to its almost zero-cost feedstock and the resulting reduction of environment burdens.[29-31] Outstanding ORR catalysts should generally have a large specific surface area, proper porosity (e.g., hierarchical meso-micro pores), and heteroatom doping (e.g., N doping).[32-37] However, owing to the intrinsic nature of waste biomass (e.g., poor porosity, a generally low N content), its carbon products without special treatment typically lacks these much-needed properties. Various carbon activation methods have been proposed to address this,[38-43] and of the NH_3 activation is regarded as one of the most effective treatment methods.[44-47] In the activation process, NH_3 etches the carbon to create pores and also covalently introduces N into the carbon molecular structure.[48, 49] Despite the improvement in ORR activity, this method still suffers from drawbacks, such as (a) the potential danger of using NH_3 gas, particularly in large-scale production, (b) the relatively time- and energy- consuming pre-treatment process required before NH_3 activation (i.e., a hydrothermal process with freeze drying or high-temperature carbonization), and (c) the C conversion efficiency of the waste biomass is relatively low, so the level of resource recovery is not satisfactory.

[a.] *Environmental Engineering Research Centre, Department of Civil Engineering, The University of Hong Kong, Pokfulam, Hong Kong, China. Email: xlia@hkucc.hku.hk, Fax: (852) 2559 5337, Tel: (852) 2859 2659.*
[b.] *School of Metallurgy and Environment, Central South University, Changsha, China.*
Electronic Supplementary Information (ESI) available: [details of any supplementary information available should be included here]. See DOI: 10.1039/x0xx00000x

In this study, we developed a new method of catalysis carbonization at a relatively low temperature, to obtain a hierarchical porous carbon as a metal-free ORR catalyst using waste biomass as the carbon source. Banana peel, which has been commonly used as a model waste biomass,[50] was selected as the carbon source for the present synthesis and experiments. This new process involves 10 min carbonization and 15 min cooling. It is simple, low-cost, efficient, and can be readily applied on a large scale with a high C conversion efficiency. The porous carbon was N-doped by melamine modification at a high temperature to create an excellent metal-free ORR catalyst. The catalyst also exhibited an outstanding methanol tolerance. The new technology can be readily used as well to produce high-performance catalysts from other typical biomass wastes, such as orange peel, leaves, etc., suggesting its potential of extensive applications.

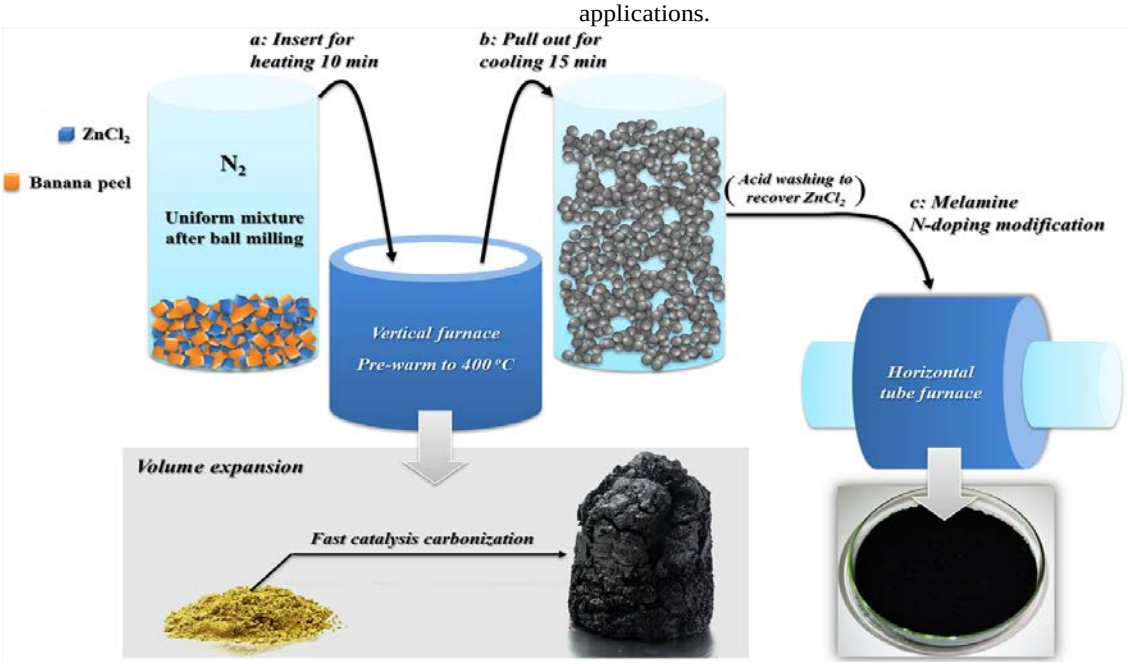

Fig. 1 Illustration of the synthesis process of hierarchical porous carbon and its N-doped product: (a) Uniform mixture of banana peel and $ZnCl_2$, prepared by ball milling followed by rapid catalysis carbonization, (b) Rapid cooling of the product, and (c) N doping by melamine modification.

2. Experimental

Materials. Zinc chloride anhydrous (98%), ethanol absolute (99.5%), and hydrochloric acid (36%) were purchased from Alfa. Melamine (99%) was obtained from Aladdin. Bananas and oranges were purchased from a local Hong Kong supermarket as the source of peel. Tea leaves were obtained after drinking tea, and tree leaves collected from the campus of the University of Hong Kong. Unless otherwise specified, the water used in the laboratory experiments was deionized water.

Production of hierarchical porous carbon from banana peel. The banana peel was washed in water to remove any dirt. The peel was then cut into pieces and dried at 105°C in an oven to provide a constant weight. The dried peel was mixed with $ZnCl_2$ powder at a weight ratio of 1:5, the $ZnCl_2$ was utilized as a catalyst for rapid carbonation. The mixture was then processed by ball milling, with the milling time and rate controlled at 30 min and 500 rpm, respectively. The uniform powders were placed into a quartz bottle filled with N_2. As illustrated in Fig. 1, the bottle was rapidly inserted into a vertical furnace that had been heated to a pre-determined temperature. After 10 min, the bottle was removed and immediately immersed into water for rapid cooling. The cooling time was 15 min. The carbon product was rinsed in HCl solution and water to remove and recover the $ZnCl_2$, and was then dried at 70°C in an oven. The carbon obtained from the fast catalysis carbonization was labeled as CZn_{rapid}-X, where X represents the temperature of the furnace. Carbon was also synthesized by the same carbonization process without using $ZnCl_2$, and the product labeled as C_{rapid}-X.

N doping of the hierarchical porous carbon. The dried carbon was thoroughly mixed with melamine at a weight ratio of 1:10. The mixture in a porcelain boat was placed into a horizontal tube furnace for heating at a specific temperature with a ramp rate of 5°C min^{-1} and an isothermal time of 2 h. The N doping process with melamine for carbon activation was protected by N_2 gas. The temperature then dropped naturally under ambient conditions. The carbon after N doping was labeled as CZn_{rapid}-X-Melamine-Y, where Y represents the activation temperature. For comparison, the carbon product without treatment with melamine for N doping was denoted as CZn_{rapid}-X-Y. The C conversion efficiency of the aforementioned process was calculated using the following equation.

$$E_c = \frac{M_{final} \times C_{final}}{M_{raw} \times C_{raw}} \times 100\ \% \quad (1)$$

where E_c is the C conversion efficiency (%), M_{final} and M_{raw} are the weights of the final carbon product and the raw material (banana peel) (g), respectively, C_{final} and C_{raw} are the C mass percentage of the final carbon product and the raw material (wt.%), respectively. The C mass ratio of the sample was obtained by the elemental analysis described below. The C mass percentage of banana peel (C_{raw}) was determined to be 43.67%.

Comparative carbonization experiment. In this study, other typical carbonization methods[40, 47, 48, 51] were also applied to prepare the carbon using banana peel. The synthesis process was the same as reported except for the raw material. The C conversion efficiency was also calculated.

Characterizations. The morphology of the samples was analyzed by a field-emission scanning electron microscope (SEM/Hitachi S4800 FEG) and a transmission electron microscope (TEM/FEI Tecnai G2). The accelerating voltage of SEM and TEM was set to be 20 and 200 kV, respectively. The specific surface area and pore size distribution of the samples were measured by the Micromeritics ASAP 2020 accelerated surface area and porosimetry system. For the measurement, the sample was degassed at 100°C for 24 h and the test was carried out at -196°C. X-ray photoelectron spectroscopy (XPS/ESCALAB 250Xi) was used to investigate the chemical composition of the samples. The vacuum degree was maintained at 5×10^{-10} mbar. In data processing, all binding energies were referenced to the C1s neutral carbon at 284.6 eV to compensate for the surface charging effect.[52] The test was conducted in air in a temperature range of 25-800°C. The quantitative content (mass percentage) of C and N of the samples was measured by the Vario Macro cube elemental analyzer. Raman scattering spectra of the samples were obtained by using the inVia confocal Raman microscope in the range of 500-4000 cm^{-1}. The acquisition time was 10 s and the He-Le laser excitation wavelength was 532 nm.

Oxygen reduction reaction. The electrocatalytic activity of the carbon products for ORR was determined by an electrochemical workstation (Solartron 1470E) using a rotating disk electrode (PINE) at room temperature. Four mg of the sample and 40 µL of 5wt.% Nafion solution were dispersed in 1 mL of ethanol followed by 40 min sonication to obtain a uniform ink. The working electrode was prepared by drop-casting 5 µL of the catalyst ink onto the glassy carbon (loading ~0.1 mg cm^{-2}). An Ag/AgCl with saturated KCl and a spiral Pt wire electrode were used as a reference electrode and counter electrode, respectively. The linear sweep voltammetry (LSV) measurements were operated in the potential range of +0.2 to -1.0 V with a scan rate of 5 mV s^{-1}, at a rotation speed varying from 400 to 2500 rpm, in the O_2-saturated 0.1 M KOH aqueous solution. The cyclic voltammogram (CV) curves were acquired in the same potential range as the LSV, using a scan rate of 50 mV s^{-1} in the O_2- or N_2- saturated 0.1 M KOH.

To further analyze the ORR potential of the catalyst, rotating ring disk measurement was performed. The record of the ring current and disk current was used to calculate the electron transfer number and the percentage of HO_2^- using the following equations.

$$\%HO_2^- = 200 \times \frac{I_r/N}{I_d + I_r/N} \quad (2)$$

$$n = 4 \times \frac{I_d}{I_d + I_r/N} \quad (3)$$

where I_d is the disk current, I_r is the ring current, and N is the current collection efficiency of the Pt ring. The N value was determined to be 0.40 from the reduction of $K_3Fe[CN]_6$.[53-56]

3. Results and discussion

3.1. Production of N-doped hierarchical porous carbon

The main steps of the carbonization and N-doping process are illustrated in Fig. 1, and consist of ball milling of the raw materials, fast carbonization followed by rapid cooling, and N doping. To achieve an effective carbonization, Zn Cl_2 was used as the catalyst, and the mixture of banana peel and $ZnCl_2$ in the quartz bottle was directly inserted into the vertical furnace pre-heated to 400°C (Fig. 1a). Within only 10 mins, the volume of the dark yellow mixture expanded dramatically after carbonization (Fig. 1a). In contrast, the conventional carbonization step would require more than 8 h (Table 1). Thus, the study presented a highly efficient and simple process for catalysis carbonization of waste biomass. The vessel for heating can also be directly taken out of the furnace for rapid cooling (15 min, Fig. 1b), while in the more typical conventional procedure the furnace has to be turned off and several hours are needed for cooling. The carbonization furnace can therefore be operated almost continuously in the new process. This will allow a simple scaling up of the system for large-scale production. The porous carbon product was well activated by N-doping with melamine at 1000°C for 2 h (Fig. 1d). It should be noted that no solid product can be obtained by the pyrolysis of pure melamine below 700°C,[57-59] and melamine decomposes into active species to incorporate N into the carbon structures at a high temperature.[60, 61] During the activation process, melamine sublimating at a high temperature will deposit as the temperature drops. This effectively avoids the potential release of unreacted melamine into the environment, and is considerably safer than using NH_3 for activation.

Table 1. Comparison of the process, nitrogen sources, yield, C content, and C conversion efficiency of the carbon products by the new method and other typical methods reported in the literature.

Methods	Time (key process)	Nitrogen sources	$M_{final}/M_{raw\ mater}$ [d]	C content (wt.%)	C conversion (%)
[a] Gradual heating & NH_3 activation	~8.6 h (gradual heating)	NH_3 (gas)	0.033	55.4	4.2
[b] Hydrothermal & NH_3 activation	~18 h (hydrothermal carbonization)	NH_3 (gas)	0.127	61.6	17.9

[c] Current method without $ZnCl_2$	10 min (fast carbonization)	Melamine (solid)	0.091	82.4	17.2
Current method	10 min (fast catalysis carbonization)	Melamine (solid)	0.204	89.7	41.9

[a, b] Detailed information can be found in *Experimental - Comparative experiment*.
[c] $ZnCl_2$ was not added in the fast carbonization step.
[d] M_{final} represents the mass of the final carbon product (g) and $M_{raw\ mater}$ represents the mass of the raw materials (g).

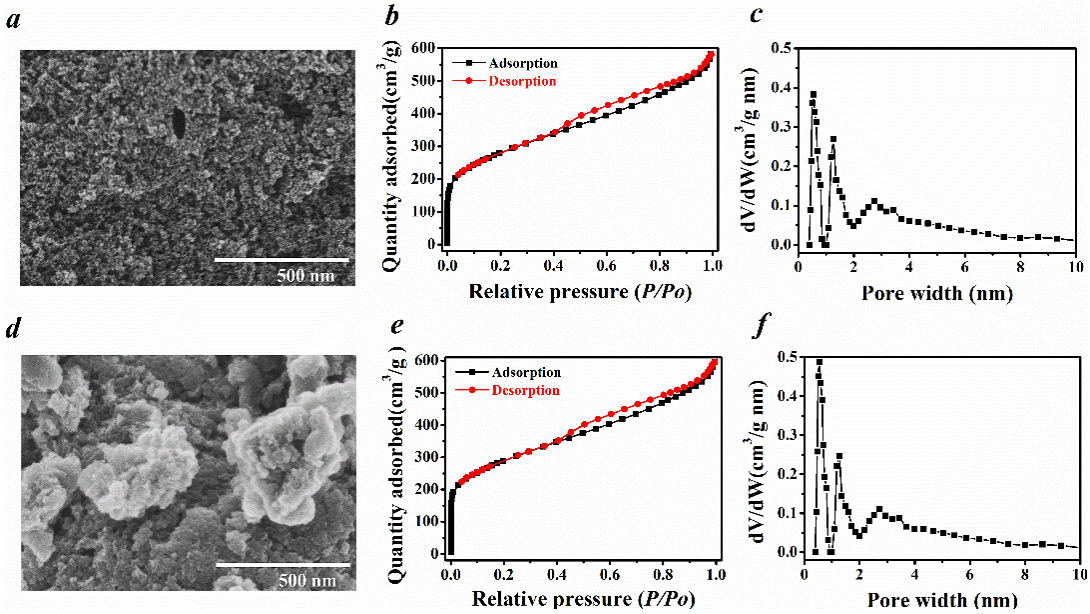

Fig. 2 SEM images of (a) CZn_{rapid}-400 and (d) CZn_{rapid}-400-Melamine-1000 (scale bar = 500 nm). N_2 adsorption-desorption isotherms of (b) CZn_{rapid}-400 and (e) CZn_{rapid}-400-Melamine-1000. Pore size distributions of (c) CZn_{rapid}-400 and (f) CZn_{rapid}-400-Melamine-1000.

The new catalysis carbonization process can also achieve a high C conversion efficiency compared to other previously reported methods. As shown in Table 1, the C conversion efficiency of CZn_{rapid}-400-Melamine-1000 reached as high as 41.9%. However, without using $ZnCl_2$ as the catalyst media for carbonization, the C conversion efficiency of C_{rapid}-400-Melamine-1000 drops to 17.2%. By the typical conventional carbonization process, the C conversion efficiency of the obtained product was less than 31% for the banana peel. The results clearly verify the outstanding resource recovery capability of the new technology developed in the present study.

3.2. Characterizations

SEM was applied to investigate the morphology of the waste biomass-derived carbon (Fig. 2). CZn_{rapid}-400 exhibits a highly porous microarchitecture, containing mesopores (<50 nm) and macropores (>50 nm) according to the SEM images (Fig. 2a). The mesopores range from 15 to 30 nm, and this porosity is typically formed by the accumulation of carbon nanoparticles. The SEM results can be further confirmed by the TEM analysis (ESI-1). Without $ZnCl_2$, the carbon products (e.g., C-400) are hardly porous (ESI-2). It is well known that $ZnCl_2$ easily evaporates or sublimates at a high temperature (typically ≥ 600 °C). Therefore, the common $ZnCl_2$-based method of making porous carbon (i.e., gradual heating to ~700°C, isothermal period ≥ 1 h)[51] often suffers from problems such as a low efficiency and a high potential of pollution and corrosion, which has been effectively avoided in the present process at a lower temperature for a short period of time. As shown in Fig. 2d, however, the numbers of mesopores (15-30 nm) of the carbon after melamine activation (CZn_{rapid}-400-Melamine-1000) declined compared to CZn_{rapid}-400, which may be due to the fusion of the pristine fine carbon nanoparticles induced at a high temperature. For further verification, CZn_{rapid}-400 was directly carbonized at 1000°C without using melamine (CZn_{rapid}-400-1000) and a similar fusion phenomenon was also observed for the carbon sample obtained (ESI-3). Melamine does not, as expected, carbonize throughout the process, but functions as a modification agent only. In fact, no carbon product can be obtained when heating melamine to 700°C in N_2. The C conversion efficiency of CZn_{rapid}-400-Melamine-1000 (20.4%) is somewhat lower than that of CZn_{rapid}-400-1000 (23.8%, Table 1), which further suggests that melamine was not involved in the carbonization but in the modification of the product. The carbon obtained at a different temperature appears to have a similar morphology as that shown in Fig. 2, produced at 400°C (ESI-4).

Figs. 2b and 2e show the N_2 adsorption-desorption isotherm of CZn_{rapid}-400 and CZn_{rapid}-400-Melamine-1000, respectively. Both of these samples display type-II isotherms with a type H3 hysteresis loop in the IUPAC classification. This type of isotherm indicates the formation of slit-shaped pores in the samples, which is in line with the nanoparticles-accumulated-structures observed with the SEM. The specific surface area of CZn_{rapid}-400 (~977 $m^2\ g^{-1}$) is slightly smaller than that of CZn_{rapid}-400-Melamine-1000 (~1009 $m^2\ g^{-1}$). The porosity, based on the Barrett-Joyner-Halenda (BJH) method, verifies the prevalence of micropores and a relatively small amount of mesopores (~4 nm), which are in agreement with Figs. 2c and 2f that reveal a hierarchical porous structure. For these two

samples, more than 85% of the surface area originates from the micropores. The micropore content typically increased after the melamine modification, which may be the main reason for the higher surface area of CZn_{rapid}-400-Melamine-1000. The N_2 adsorption-desorption isotherm and pore size distribution of CZn_{rapid}-400-Melamine-900/1100 are given in ESI-5, which both exhibit similar physiochemical properties to CZn_{rapid}-400-Melamine-1000. Generally speaking, the porosity analysis further proves the effectiveness of the new carbonization method in producing highly porous carbon with a favorable hierarchical porous structure.

XPS detection results of CZn_{rapid}-400 and CZn_{rapid}-400-Melamine-900/1000/1100 are provided in Fig. 3. The C1s high-resolution spectra of these four products show two dominant peaks at ~284.3 and ~284.8 eV, which correspond to the sp^2 hybridized graphitized carbon (C1) and sp^3 C-C carbon (C2), respectively. The two other weak peaks at ~285.7 and ~286.8 eV are attributable to C-O/C-N (C3) and C=O (C4), respectively. The content of C1 clearly increases with the increase in N-doing temperature, suggesting its improvement in conductivity. In the N1s high-resolution spectra, pyridinic (N1), amine/imine (N2), pyrrolic (N3), quaternary (N4), and pyridinic-N-oxide (N5) can be detected, which confirms that the N doping of the carbon materials and N1 and N3 account for more than 65 at.% of the total N content in the products. Though the amount of N in carbon decreased with the temperature increase, it still reached ~3 at.% even after the melamine modification at 1100°C.

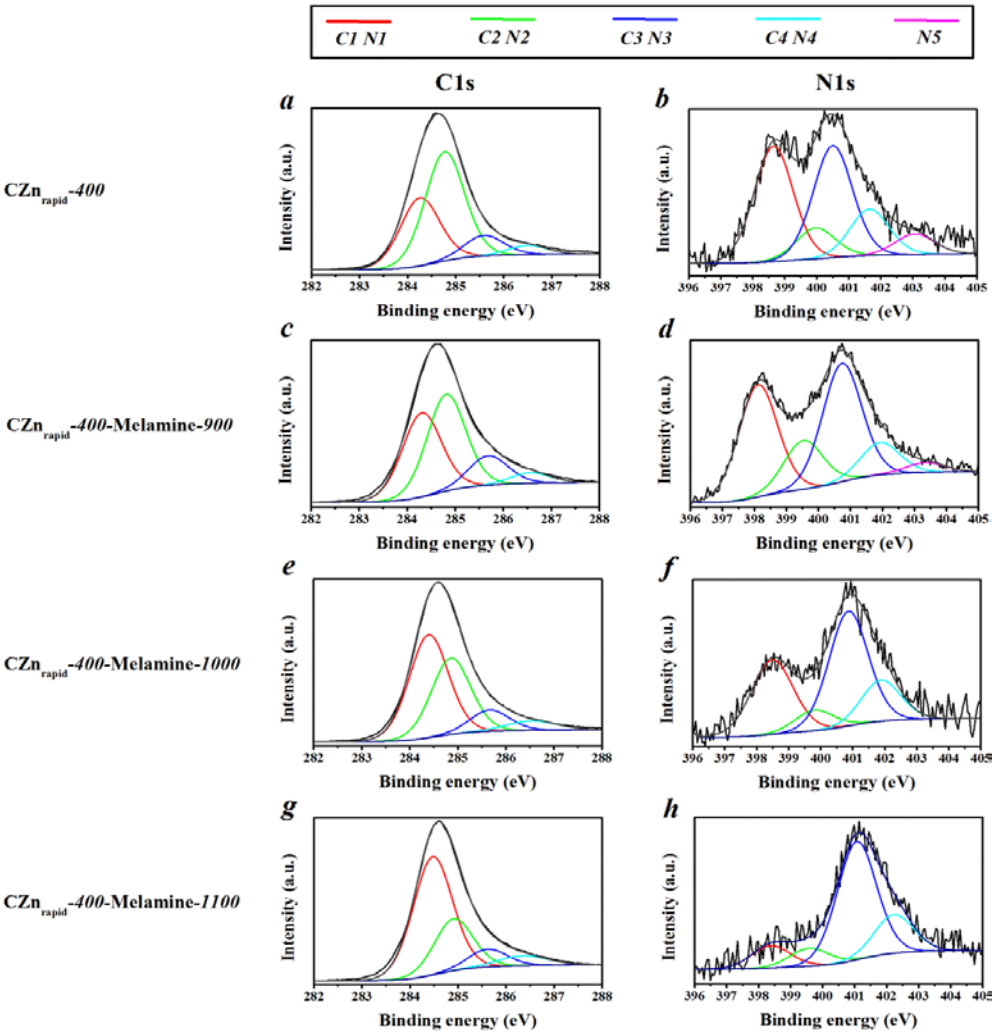

Fig. 3 High-resolution C1s (a, c, e, g) and N1s (b, d, f, h) XPS spectra of the carbon products: CZn_{rapid}-400, CZn_{rapid}-400-Melamine-900, CZn_{rapid}-400-Melamine-1000, and CZn_{rapid}-400-Melamine-1100. The color of the lines in the Figure represents specific C or N species. C1: sp2 hybridized graphitized carbon, C2: sp3 C-C carbon, C3: C-O or C-N, C4: C=O; N1: pyridinic-N, N2: amine or imine, N3: pyrrolic N, N4: quaternary N, N5: pyridinic-N-oxide.

Table 2. Summary of the chemical composition analysis based on high-resolution XPS spectra. The representation of *N1-N5* and *C1-C2* is given in the caption of Fig. 3.

	Nx:N (%) [a]					*Cx:C (%)* [b]	
Sample	*N1*	*N2*	*N3*	*N4*	*N5*	*C1*	*C2*
CZn_{rapid}-*400*	35.48	9.51	34.47	14.20	6.33	32.90	52.79

CZn_{rapid}-*400*-Melamine-*900*	34.89	15.18	36.84	10.07	3.02	38.43	43.43
CZn_{rapid}-*400*-Melamine-*1000*	31.09	8.01	44.86	16.04	-[c]	48.44	35.94
CZn_{rapid}-*400*-Melamine-*1100*	11.31	9.00	60.06	19.63	-[c]	59.86	25.90

[a] *Nx*:*N* is the relative molar ratio of the specific N species to the total N.

[b] *Cx*:*C* is the relative molar ratio of the specific C species to the total C.

[c] *N5* cannot be detected in CZn_{rapid}-*400*-Melamine-*1000*/*1100*.

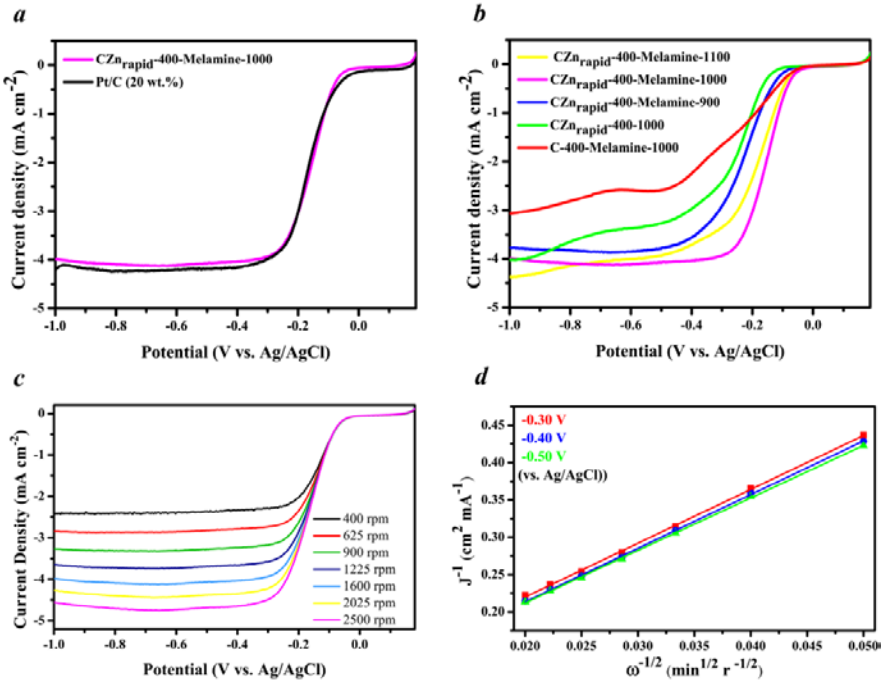

Fig. 4 LSV curves for (a) CZn_{rapid}-400-Melamine-1000 and commercial Pt/C in O_2-saturated KOH solution at a rotation rate of 1600 rpm, (b) various samples in O_2-saturated 0.1 M KOH at a rotation rate of 1600 rpm, and (c) CZn_{rapid}-400-Melamine-1000 at different rotation rates in O_2-saturated 0.1 M KOH solution at a scan rate of 5 mV s^{-1}; and (d) K–L plot of CZn_{rapid}-400-Melamine-1000 derived from (c).

The samples were also characterized by the Raman spectra (ESI-6). For CZn_{rapid}-400-Melamine-900/1000/1100, there is a D band at ~1350 cm^{-1} and a G band at ~1600 cm^{-1}, and a broad 2D peak at ~2700 cm^{-1}, suggesting good graphitization results for these carbon products.

3.3. Electrocatalytic activity

To evaluate the electrocatalytic activity of the N-doped porous carbon, linear sweep voltammetry (LSV) was conducted and commercial Pt/C used as a benchmark material (Fig. 4). Fig. 4a shows that CZn_{rapid}-400-Melamine-1000 exhibits a similar onset potential and reduction current for ORR as Pt/C, revealing a comparable electrocatalytic activity. This can contribute to the synergetic effect of the good conductivity, hierarchical porosity, and high N doping level of the carbon. For the carbon produced under various experimental conditions, including the use of $ZnCl_2$ and different temperatures for carbonization, CZn_{rapid}-400-Melamine-1000 shows the optimum performance (Fig. 4b and ESI-7). In addition, the important effect of N doping on the catalytic activity is verified by comparing the CZn_{rapid}-400-Melamine-1000 with CZn_{rapid}-400-1000 (Fig. 4b). The onset potential of CZn_{rapid}-400-Melamine-1000 is 82 mV higher than that of CZn_{rapid}-400-1000. The fabrication of metal-free catalysts has been developed in recent years,[25, 58, 62-64] but the catalysts reported are still found to have considerably weak electrocatalytic activities compared to commercial 20% Pt/C in alkaline media. More recently, a general carbonization method based on NH_3 activation has been proposed to produce Pt-comparable catalysts.[44-49] However, as shown above for a comparative test and product, this method is much more time-consuming and has a relatively low C recovery efficiency compared to the new carbonization and activation method developed in the present work. Metal-free catalysts synthesized with banana peel have also been reported.[47, 48]. As presented in ESI-8, the ORR catalytic performance of all these carbon products is inferior to CZn_{rapid}-400-Melamine-1000. The comparison indicates the superiority of the new method in fabricating high-performance, metal-free ORR catalysts.

The LSV curves in Fig. 4c reveal an obvious increase of current density at an increasing rotation rate, which can be ascribed to the shorter diffusion route. Fig. 4d is derived from Fig. 4c based on the Koutecky-Levich (K-L) equation,[55, 65] as below:

$$\frac{1}{J} = \frac{1}{J_K} + \frac{1}{J_L} = \frac{1}{B\omega^{\frac{1}{2}}} + \frac{1}{J_K} \quad (4)$$

$$B = 0.2nF(D_0)^{\frac{2}{3}}\nu^{-\frac{1}{6}}C_0 \quad (5)$$

where J_K stands for the kinetic current density, J_L is the limited diffusion current density, ω represents the RDE rotation rate (rpm), F is the Faraday constant (96485 C mol^{-1}), D_0 is the diffusion coefficient and the bulk O_2 concentration is denoted as C_0, υ is the kinetic viscosity of the electrolyte, and B can be acquired from the slope of the fitting line. Based on the K-L equation, n (electron transfer number) can be calculated from the B value. The oxygen reduction process is mainly directed by a four-electron pathway ($O_2+2H_2O+4e^-=4OH^-$), which is consistent with the analysis of K-L plots.[66]

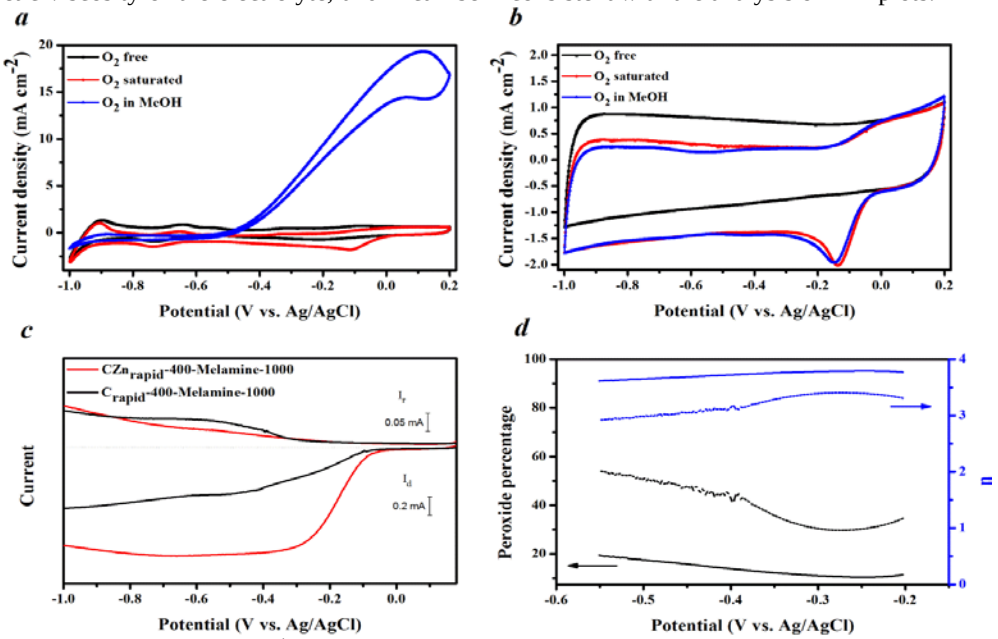

Fig. 5 CV curves for the ORR at 50 mV s^{-1} for (a) commercial Pt/C (20 wt.%) catalyst and (b) CZn_{rapid}-400-Melamine-1000 at different conditions; (c) Rotating ring-disk electrode voltammograms for the ORR at the CZn_{rapid}-400-Melamine-1000 and C_{rapid}-400-Melamine-1000 in O_2-saturated 0.1 M KOH solution at 1600 rpm, the disk current (I_d) is shown on the lower half of the graph and the ring current (I_r) on the upper half; and (d) The percentage of peroxide (black line) and the electron transfer number (n) (blue line) of CZn_{rapid}-400-Melamine-1000 (solid line) and C_{rapid}-400-Melamine-1000 (dashed line) at various potentials, based on the corresponding RRDE data in (c).

The poor tolerance of noble metal catalysts to methanol is one of the biggest challenges in the application of fuel cells. For the carbon catalysts obtained in the present study, their resistance to methanol oxidation was evaluated by measuring the CV curves operated in the O_2-saturated KOH solution with 3 M methanol. Fig. 5a shows a pair of peaks at 0.12 and 0.16 V, which can be assigned to the methanol oxidation reaction of Pt/C, while in Fig. 5b, scarcely any change can be observed for CZn_{rapid}-400-Melamine-1000 in the methanol and common conditions. Thus, the as-prepared carbon possesses a better methanol-tolerance ability than the commercial Pt/C. The CV curves tested in the N_2- and O_2-saturated KOH solution clearly show the O_2 reduction peak in the potential range.

To further understand the ORR electron transfer route by CZn_{rapid}-400-Melamine-1000, a rotating ring-disk electrode (RRDE) measurement was carried out and subsequently the production of HO_2^- in oxygen reduction process was analyzed. The ring and disk currents were measured to obtain the HO_2^- yield in the reaction (Fig. 5c). The recorded HO_2^- percentages of CZn_{rapid}-400-Melamine-1000 and C_{rapid}-400-Melamine-1000 in 0.1 M KOH are below 20% and 50%, respectively, in the potential range of -0.55 V to -0.2 V, corresponding with the electron transfer numbers of ~3.7 and ~3.3 (Fig. 5d). The values calculated from the K-L plot of CZn_{rapid}-400-Melamine-1000 coincide well with the RRDE result, which confirms the four-electron transfer route by CZn_{rapid}-400-Melamine-1000 for the ORR process.

Fig. 6a shows that the CV curve of CZn_{rapid}-400-Melamine-1000 in the first cycle overlaps perfectly with the 2000th cycle, demonstrating its excellent durability in alkaline solution. The stability of Pt/C in 0.1 M KOH was also evaluated to confirm the superiority of CZn_{rapid}-400-Melamine-1000 for the potential application in fuel cells for long-term operation. In Fig. 6b, the CV curves of Pt/C for the first cycle and the 2000th cycle are less consistent with each other, indicating that the durability of the commercial product is not better than that of CZn_{rapid}-400-Melamine-1000.

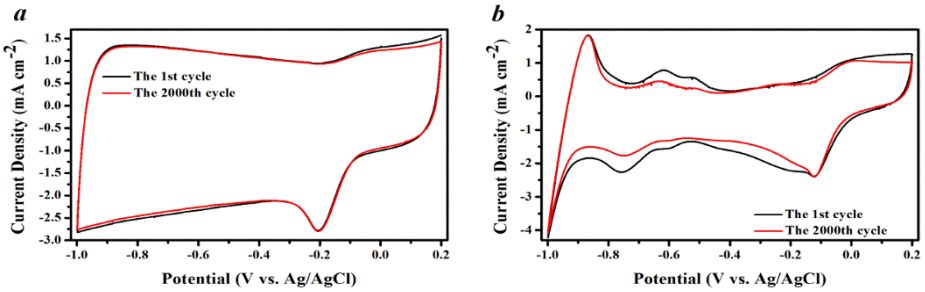

Fig. 6 The 1st and the 2000th CV curves of (a) CZn_{rapid}-400-Melamine-1000 and (b) commercial Pt/C with a scan rate of 100 mV s^{-1} in O_2-saturated 0.1 M KOH solution.

The outstanding ORR performance of the N-doped porous carbon should be related to its intrinsic properties, in which proper nitrogen doping and high porosity are two important factors (Scheme 1). The N doping promotes the reactivity of the carbon material, particularly the pyridinic and pyrrolic N,[67] while the hierarchical porous structures are beneficial for mass transportation. Most importantly, the high content of micropores provides a large specific surface area to accommodate the N active sites reacting with O_2. Micropores provide ideal sites for the ORR reaction.[47] In the present research, CZn_{rapid}-400-Melamine-1000 possesses a high content of active N species and the highest content of micropores, and is therefore a better ORR catalyst than the other four samples prepared at different temperatures. Apart from these two property factors, the good conductivity of the carbon, as deduced from the XPS and Raman characterizations, is also essential.

Scheme 1. Proposed ORR catalytic process by the N-doped porous carbon.

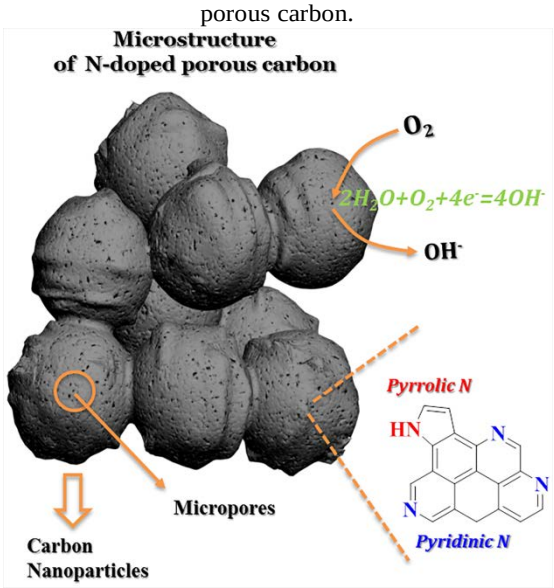

The generality of the new carbonization technique was further verified with different biomass as the carbon sources. Orange peel and leaves were selected for the additional experiments. As illustrated in ESI-9, their corresponding carbon materials also exhibited excellent catalytic activities, which are close to those of commercial Pt/C. It should be noted that the production conditions of these carbon materials are identical to those for CZn_{rapid}-400-Melamine-1000. The test results demonstrate the high level of effectiveness of our new method, which can be widely applied to synthesize superior carbon catalysts using a variety of raw waste biomass materials.

The new method consists of two main steps: fast $ZnCl_2$ catalysis carbonization and melamine modification. Biomass-derived catalysts produced by one-step $ZnCl_2$-activated carbonization under a heating condition have also been reported.[51] However, the generality of the one-step process is questionable and the products less reproducible, as the N activation result is significantly affected by the original N content in the raw materials,[68] which varies greatly between different natural biomass materials. For example, when applying lignin, HNO_3 must be used to introduce the N group into the feedstock before $ZnCl_2$ activation.[69] In the present study, a comparative test was conducted using the one-step $ZnCl_2$ carbonization and activation of banana peel. As shown in ESI-10, the ORR catalytic activity of the product is clearly weaker than CZn_{rapid}-400-Melamine-1000, and also of Pt/C. Besides its poor generality and poor quality control, one-step $ZnCl_2$ activation is commonly conducted at a high temperature with a long isothermal period. This inevitably leads to a low production efficiency and strong evaporation and sublimation of $ZnCl_2$ during the process, causing potential equipment corrosion and environmental pollution.

Conclusions

N-doped hierarchical porous carbon derived from banana peel is successfully synthesized by fast catalysis carbonization at 400°C and melamine modification at 1000°C, which possesses a high surface area (>1000 m^2 g^{-1}), abundant micropores, and relatively high N content. The whole process of fast catalysis carbonization can be shortened to less than 30 min and the operation becomes semi-continuous, which would allow for large-scale production. The C conversion efficiency can reach as high as 41.3%, achieving effective resources recovery. The N-doped porous carbon exhibits an outstanding ORR activity in an alkaline medium and much better methanol tolerance compared to commercial Pt/C. The high surface area, well-developed micropores, and high content of pyridinic and pyrrolic N together contribute to the excellent ORR activity of the carbon product. Promising metal-free ORR catalysts can also be produced from other waste biomass (e.g., orange peel,

leaves). The research presents an effective, low-cost, and generally scalable approach for fabricating waste biomass-derived carbon, with a hierarchical porous structure, heteroatom doping, and high activities. Such a development will be essential to the applications of porous carbon in the areas of energy conversion and storage.

Acknowledgements

We acknowledge the funding support from The Research Grants Council of Hong Kong: Collaborative Research Fund (C7044-14G) and Theme-based Research Scheme (T21-711/16R).

Notes and references

1. E. Antolini, *Appl. Catal., B*, 2016, **181**, 298-313.
2. X. Luo, J. Wang, M. Dooner and J. Clarke, *Appl. Energy*, 2015, **137**, 511-536.
3. D. Larcher and J. M. Tarascon, *Nat. Chem.*, 2015, **7**, 19-29.
4. C. Zhu, H. Li, S. Fu, D. Du and Y. Lin, *Chem. Soc. Rev.*, 2016, **45**, 517-531.
5. G. Ren, G. Ma and N. Cong, *Renewable Sustainable Energy Rev.*, 2015, **41**, 225-236.
6. Y. Zheng, Y. Jiao, M. Jaroniec, Y. Jin and S. Z. Qiao, *Small*, 2012, **8**, 3550-3566.
7. X. Ge, A. Sumboja, D. Wuu, T. An, B. Li, F. W. T. Goh, T. S. A. Hor, Y. Zong and Z. Liu, *ACS Catalysis*, 2015, **5**, 4643-4667.
8. G. A. Ferrero, K. Preuss, A. Marinovic, A. B. Jorge, N. Mansor, D. J. Brett, A. B. Fuertes, M. Sevilla and M. M. Titirici, *ACS nano*, 2016, **10**, 5922-5932.
9. L. Xiong, J.-J. Chen, Y.-X. Huang, W.-W. Li, J.-F. Xie and H.-Q. Yu, *Nano Energy*, 2015, **12**, 33-42.
10. L. Li, C. Liu, G. He, D. Fan and A. Manthiram, *Energy Environ. Sci.*, 2015, **8**, 3274-3282.
11. N. Cheng, M. N. Banis, J. Liu, A. Riese, X. Li, R. Li, S. Ye, S. Knights and X. Sun, *Adv. Mater.*, 2015, **27**, 277-281.
12. D. Li, C. Wang, D. S. Strmcnik, D. V. Tripkovic, X. Sun, Y. Kang, M. Chi, J. D. Snyder, D. van der Vliet, Y. Tsai, V. R. Stamenkovic, S. Sun and N. M. Markovic, *Energy Environ. Sci.*, 2014, **7**, 4061-4069.
13. X. Huang, Z. Zhao, Y. Chen, E. Zhu, M. Li, X. Duan and Y. Huang, *Energy Environ. Sci.*, 2014, **7**, 2957.
14. D. Geng, N. Ding, T. S. Andy Hor, Z. Liu, X. Sun and Y. Zong, *J. Mater. Chem. A*, 2015, **3**, 1795-1810.
15. L. Dai, Y. Xue, L. Qu, H. J. Choi and J. B. Baek, *Chemical Reviews*, 2015, **115**, 4823-4892.
16. W. He, Y. Wang, C. Jiang and L. Lu, *Chem. Soc. Rev.*, 2016, **45**, 2396-2409.
17. M. Zhou, H. L. Wang and S. Guo, *Chem. Soc. Rev.*, 2016, **45**, 1273-1307.
18. L. Tao, Q. Wang, S. Dou, Z. Ma, J. Huo, S. Wang and L. Dai, *Chemical Communications*, 2016, **52**, 2764-2767.
19. J. Wang, L. Li, X. Chen, Y. Lu and W. Yang, *J. Mater. Chem. A*, 2016, DOI: 10.1039/c6ta03518c.
20. Y. Zhao, L. Yang, S. Chen, X. Wang, Y. Ma, Q. Wu, Y. Jiang, W. Qian and Z. Hu, *J. Am. Chem. Soc.*, 2013, **135**, 1201-1204.
21. T. Zhou, Y. Du, S. Yin, X. Tian, H. Yang, X. Wang, B. Liu, H. Zheng, S. Qiao and R. Xu, *Energy Environ. Sci.*, 2016, **9**, 2563-2570.
22. K. Gong, F. Du, Z. Xia, M. Durstock and L. Dai, *Science*, 2009, **323**, 760-764.
23. C. Guo, W. Liao, Z. Li, L. Sun and C. Chen, *Nanoscale*, 2015, **7**, 15990-15998.
24. P. Ayala, R. Arenal, M. Rümmeli, A. Rubio and T. Pichler, *Carbon*, 2010, **48**, 575-586.
25. S. Chen, J. Bi, Y. Zhao, L. Yang, C. Zhang, Y. Ma, Q. Wu, X. Wang and Z. Hu, *Adv. Mater.*, 2012, **24**, 5593-5597, 5646.
26. S. Lee, M. Choun, Y. Ye, J. Lee, Y. Mun, E. Kang, J. Hwang, Y. H. Lee, C. H. Shin, S. H. Moon, S. K. Kim, E. Lee and J. Lee, *Angew. Chem. Int. Ed.*, 2015, **54**, 9230-9234.
27. G. Wang, Y. Sun, D. Li, H. W. Liang, R. Dong, X. Feng and K. Mullen, *Angew. Chem. Int. Ed.*, 2015, **54**, 15191-15196.
28. S. Yang, X. Feng, X. Wang and K. Mullen, *Angew. Chem. Int. Ed.*, 2011, **50**, 5339-5343.
29. S. J. Yuan and X. H. Dai, *Sci. Rep.*, 2016, **6**, 27570.
30. S. Gao, L. Li, K. Geng, X. Wei and S. Zhang, *Nano Energy*, 2015, **16**, 408-418.
31. J. Zhang, Q. Li, C. Zhang, L. Mai, M. Pan and S. Mu, *Electrochim. Acta*, 2015, **160**, 139-144.
32. J. Yang, H. Sun, H. Liang, H. Ji, L. Song, C. Gao and H. Xu, *Adv. Mater.*, 2016, **28**, 4606-4613.
33. K. Qiu, G. Chai, C. Jiang, M. Ling, J. Tang and Z. Guo, *ACS Catalysis*, 2016, **6**, 3558-3568.
34. L. Zhou, P. Fu, Y. Wang, L. Sun and Y. Yuan, *J. Mater. Chem. A*, 2016, **4**, 7222-7229.
35. Y. Li, W. Zhou, H. Wang, L. Xie, Y. Liang, F. Wei, J. C. Idrobo, S. J. Pennycook and H. Dai, *Nature Nanotechnology*, 2012, **7**, 394-400.
36. S. Wang, D. Yu, L. Dai, D. W. Chang and J. B. Baek, *ACS Nano*, 2011, **5**, 6202-6209.
37. K. Qu, Y. Zheng, S. Dai and S. Z. Qiao, *Nano Energy*, 2016, **19**, 373-381.
38. H. Yu, L. Shang, T. Bian, R. Shi, G. I. Waterhouse, Y. Zhao, C. Zhou, L. Z. Wu, C. H. Tung and T. Zhang, *Adv. Mater.*, 2016, **28**, 5080-5086.
39. H. Zhang, Y. Wang, D. Wang, Y. Li, X. Liu, P. Liu, H. Yang, T. An, Z. Tang and H. Zhao, *Small*, 2014, **10**, 3371-3378.
40. S. Gao, K. Geng, H. Liu, X. Wei, M. Zhang, P. Wang and J. Wang, *Energy Environ. Sci.*, 2015, **8**, 221-229.
41. D. Mondal, M. Sharma, C.-H. Wang, Y.-C. Lin, H.-C. Huang, A. Saha, S. K. Nataraj and K. Prasad, *Green Chem.*, 2016, **18**, 2819-2826.
42. R. Wang, K. Wang, Z. Wang, H. Song, H. Wang and S. Ji, *J. Power Sources*, 2015, **297**, 295-301.
43. S.-M. Alatalo, K. Qiu, K. Preuss, A. Marinovic, M. Sevilla, M. Sillanpää, X. Guo and M.-M. Titirici, *Carbon*, 2016, **96**, 622-630.
44. S.-J. Yuan and X.-H. Dai, *Green Chem.*, 2016, **18**, 4004-4011.
45. W. Wan, Q. Wang, L. Zhang, H.-W. Liang, P. Chen and S.-H. Yu, *J. Mater. Chem. A*, 2016, **4**, 8602-8609.
46. W. Yuan, Y. Feng, A. Xie, X. Zhang, F. Huang, S. Li, X. Zhang and Y. Shen, *Nanoscale*, 2016, **8**, 8704-8711.
47. P. Chen, L.-K. Wang, G. Wang, M.-R. Gao, J. Ge, W.-J. Yuan, Y.-H. Shen, A.-J. Xie and S.-H. Yu, *Energy Environ. Sci.*, 2014, **7**, 4095-4103.
48. F. Pan, Z. Cao, Q. Zhao, H. Liang and J. Zhang, *J. Power Sources*, 2014, **272**, 8-15.
49. H. Zhou, J. Zhang, I. S. Amiinu, C. Zhang, X. Liu, W. Tu, M. Pan and S. Mu, *Phys. Chem. Chem. Phys.*, 2016, **18**, 10392-10399.
50. E. M. Lotfabad, J. Ding, K. Cui, A. Kohandehghan, W. P. Kalisvaart, M. Hazelton and D. Mitlin, *ACS Nano*, 2014, **8**, 7115-7129.
51. X. Liu, Y. Zhou, W. Zhou, L. Li, S. Huang and S. Chen, *Nanoscale*, 2015, **7**, 6136-6142.
52. L. Zhang, Y. Wang, B. Peng, W. Yu, H. Wang, T. Wang, B. Deng, L. Chai, K. Zhang and J. Wang, *Green Chem.*, 2014, **16**, 3926.
53. Y. C. Wang, Y. J. Lai, L. Song, Z. Y. Zhou, J. G. Liu, Q. Wang, X. D. Yang, C. Chen, W. Shi, Y. P. Zheng, M. Rauf and S. G. Sun, *Angew. Chem. Int. Ed.*, 2015, **54**, 9907-9910.
54. X. L. Wu, T. Wen, H. L. Guo, S. Liu, X. Wang, A. W. Xu and M. Mezger, *Sci. Rep.*, 2016, **6**, 28049.
55. Y. Liang, Y. Li, H. Wang, J. Zhou, J. Wang, T. Regier and H. Dai, *Nature Materials*, 2011, **10**, 780-786.
56. W. Yang, L. Chen, X. Liu, X. Yue, C. Liu and J. Jia, *J. Mater. Chem. A*, 2016, **4**, 5834-5838.
57. X. Huang, K. Qian, J. Yang, J. Zhang, L. Li, C. Yu and D. Zhao, *Advanced Materials*, 2012, **24**, 4419-4423.
58. J. Liang, Y. Jiao, M. Jaroniec and S. Z. Qiao, *Angewandte Chemie International Edition*, 2012, **51**, 11496-11500.
59. J. Xiao, X. Bian, L. Liao, S. Zhang, C. Ji and B. Liu, *ACS Applied Materials & Interfaces*, 2014, **6**, 17654-17660.

60. G. A. Ferrero, A. B. Fuertes, M. Sevilla and M.-M. Titirici, *Carbon*, 2016, **106**, 179-187.
61. A. B. Fuertes, G. A. Ferrero and M. Sevilla, *Journal of Materials Chemistry A*, 2014, **2**, 14439.
62. P. Chen, T.-Y. Xiao, Y.-H. Qian, S.-S. Li and S.-H. Yu, *Adv. Mater.*, 2013, **25**, 3192-3196.
63. D. Geng, Y. Chen, Y. Chen, Y. Li, R. Li, X. Sun, S. Ye and S. Knights, *Energy & Environmental Science*, 2011, **4**, 760.
64. L. Qu, Y. Liu, J.-B. Baek and L. Dai, *ACS Nano*, 2010, **4**, 1321-1326.
65. S. You, X. Gong, W. Wang, D. Qi, X. Wang, X. Chen and N. Ren, *Adv. Energy Mater.*, 2016, **6**, n/a-n/a.
66. R. Zhou, Y. Zheng, M. Jaroniec and S.-Z. Qiao, *ACS Catalysis*, 2016, **6**, 4720-4728.
67. D. Guo, R. Shibuya, C. Akiba, S. Saji, T. Kondo and J. Nakamura, *Science*, 2016, **351**, 361-365.
68. W. Yang, T.-P. Fellinger and M. Antonietti, *J. Am. Chem. Soc.*, 2011, **133**, 206-209.
69. M. Graglia, J. Pampel, T. Hantke, T. P. Fellinger and D. Esposito, *ACS Nano*, 2016, **10**, 4364-4371.